Molecular mechanism of membrane recruitment of GGA by ARF in lysosomal protein transport

Tomoo Shiba[1–3], Masato Kawasaki[1,3], Hiroyuki Takatsu[4,5], Terukazu Nogi[1,6], Naohiro Matsugaki[1], Noriyuki Igarashi[1], Mamoru Suzuki[1], Ryuichi Kato[1], Kazuhisa Nakayama[4,7] and Soichi Wakatsuki[1]

Published online 7 April 2003; doi:10.1038/nsb920

GGAs are critical for trafficking soluble proteins from the *trans*-Golgi network (TGN) to endosomes/lysosomes through interactions with TGN-sorting receptors, ADP-ribosylation factor (ARF) and clathrin. ARF–GTP bound to TGN membranes recruits its effector GGA by binding to the GAT domain, thus facilitating recognition of GGA for cargo-loaded receptors. Here we report the X-ray crystal structures of the human GGA1-GAT domain and the complex between ARF1–GTP and the N-terminal region of the GAT domain. When unbound, the GAT domain forms an elongated bundle of three α-helices with a hydrophobic core. Structurally, this domain, combined with the preceding VHS domain, resembles CALM, an AP180 homolog involved in endocytosis. In the complex with ARF1–GTP, a helix-loop-helix of the N-terminal part of GGA1-GAT interacts with the switches 1 and 2 of ARF1 predominantly in a hydrophobic manner. These data reveal a molecular mechanism underlying membrane recruitment of adaptor proteins by ARF–GTP.

Adaptor protein (AP) complexes play critical roles in vesicular transport between membrane-bound organelles by recognizing cargo receptors, and recruiting clathrin and various accessory proteins[1]. Clathrin/AP-1–coated vesicles were believed to be solely responsible for transport between the *trans*-Golgi network (TGN) and endosomes/lysosomes. However, recent identification of a novel family of adaptor proteins, called GGAs (Golgi-localizing, γ-adaptin ear homology domain, ARF-binding proteins)[2–6], has prompted re-evaluation of the molecular mechanisms of vesicle transport. The GGA molecule is composed of four major domains: the VHS (Vps27p/Hrs/STAM) domain that binds TGN sorting receptors, such as mannose 6-phosphate receptors (MPRs), sortilin and β-secretase by recognizing acidic cluster dileucine (ACLL) sequences; the GAT (GGA and Tom1) domain that interacts with GTP-bound ARF; a proline-rich hinge region that interacts with clathrin; and the GAE (γ-adaptin ear) domain that interacts with accessory proteins, such as Rabaptin-5 and γ-synergin. Further studies suggest that GGAs regulate transport of glycosylated lysosomal proteins from the TGN to the endosomes and lysosomes[7–10]. Unlike hetero-tetrameric AP complexes, GGAs function as monomers. Furthermore, an interaction between GGAs and the γ-ear domain of the AP-1 complex has been reported[11], which suggests transfer of cargo-loaded receptors between the two.

The adaptor proteins APs and GGAs need to be recruited to membrane surfaces for increased efficiency to find cargo receptors. A small GTPase, ARF, plays a crucial role in docking the adaptor proteins to membranes. Although GDP-bound ARF is cytosolic, it associates with membranes upon exchange of GDP with GTP, which can enhance the efficiency of the adaptor proteins to encounter cargo receptors, such as MPRs bound to lysosomal hydrolases. Although it is currently unclear which part of AP adaptins is responsible for the interaction with ARF–GTP, the GAT domain of GGAs has been identified as the key region of GGA that interacts with ARF–GTP and serves as a molecular anchor of GGA to TGN membranes[2,3,12–14]. However, this domain has eluded structural analyses probably because the hinge regions connecting the GGA-GAT domain with the rest of GGA are flexible and the interaction between GGAs and ARF–GTP causes a structural rearrangement of GGA (see below). We have solved the X-ray structure of the human GGA–GAT domain in complex with ARF–GTP by overcoming the problem through an extensive search of conditions for a stable complex between them.

Structure of GGA1-GAT domain

We solved the structure of the GGA1-GAT domain (residues 166–305) alone by the MAD method using a SeMet-substituted GGA1-GAT at 2.1 Å. The structure shows an elongated three-helix bundle (residues 192–303) with a hydrophobic core, in which the N-terminal helix is twice as long as the other two (Fig. 1*a*). This GAT domain preparation contains an N-terminal region (residues 166–191) upstream of the long N-terminal helix, but it is highly disordered in the crystal structure. The three-helix bundle resembles the last three helices of the ANTH (AP180 N-terminal homology) domain of CALM (clathrin assembly lymphoid myeloid leukemia protein), an AP180 homolog, which is a class of proteins involved in endocytosis[15,16]. In fact, the first six helices of CALM are structurally similar to the known VHS structures; the VHS domain of GGA indeed

[1]Photon Factory, Institute of Materials Structure Science, High Energy Accelerator Research Organization (KEK), Tsukuba, Ibaraki 305-0801, Japan. [2]Foundation for Advancement of International Science (FAIS), Tsukuba, Ibaraki 305-0062, Japan. [3]These authors have contributed equally to this work. [4]Institute of Biological Sciences and Gene Research Center, University of Tsukuba, Tsukuba, Ibaraki 305-8572, Japan. [5]Present address: RIKEN Research Center for Allergy and Immunology (RCAI), Yokohama, Kanagawa 230-0045, Japan. [6]Present address: Max-Planck-Institute of Biophysics, 60439 Frankfurt am Main, Germany. [7]Present address: Faculty of Pharmaceutical Sciences, Kanazawa University, Kanazawa, Ishikawa 920-0934, Japan.

Correspondence should be addressed to S.W. *e-mail: soichi.wakatsuki@kek.jp*

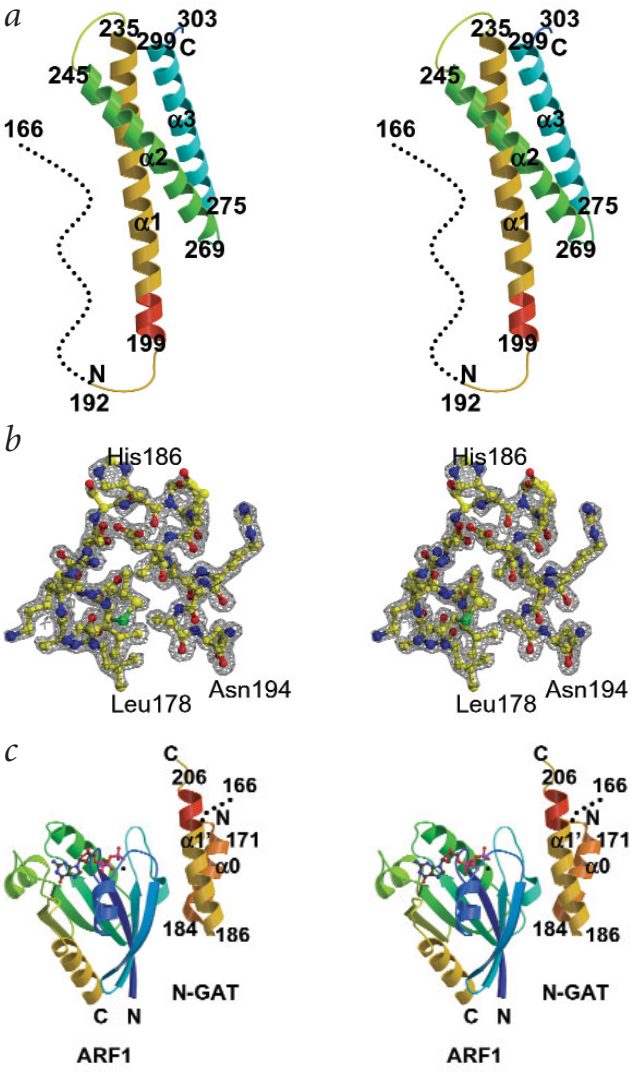

forms a right-handed super helix[17,18]. Taken together, the VHS and the GAT domains might form an overall structure similar to that of AP180 (Fig. 2). This implies that the extended super helix could be a recurrent structure used in vesicle transport. The significance of this implication, however, needs further analysis because this part of GGA recognizes the ACLL signal and ARF–GTP, whereas AP180 recognizes phosphatidylinositol-4,5-bisphosphate at a different location in the cell[15].

Fig. 2 Comparison of the GGA VHS-GAT domain with AP180 homologs. ***a***, Ribbon diagram of the N-terminal domain of CALM (PDB entry 1HG5). Helices α1–α7 are shown in blue and α9–α11 are shown in green. The inositol hexakisphosphate molecule is shown in a ball-and-stick model. ***b***, Ribbon diagram of the N-terminal domain of *Drosophila* clathrin adaptor protein LAP (PDB entry 1HX8). Helices α1–α7 are shown in blue and α9–α12 in green. ***c***, Ribbon diagram of the VHS domain of GGA1 in complex with C-terminal cation independent-M6PR (CI-M6PR) peptide (PDB entry 1JWG) in the same orientation as in (*a*). CI-M6PR peptide is shown as a ball-and-stick model. ***d***, Ribbon diagram of the GGA1-GAT domain in the same orientation as in (*a*). There are striking structural similarities between the N-terminal of CALM (*a*, α1–α7 in blue) and the VHS domain of GGA1 (*c*), and between the C-terminal of CALM (*a*, α9–α11 in green) and the GAT domain of GGA1 (*d*, α1–α3) except for the following differences. The N-terminal six α-helices of CALM, α1–α5 and α7 have two deletions of α-helices (α6 and α8) compared with the GGA1 VHS domain. In addition, the helix α7 is longer than the corresponding helix of the GGA1-VHS domain. In the GAT region, there are two short α-helix insertions in CALM (between α9 and α10, and between α11 and the C terminus), and the helix α9 of CALM is shorter than that of the GGA1-GAT domain.

Fig. 1 Structures of the GGA1-GAT domain and its complex with ARF1. ***a***, Stereo diagram of the GGA1-GAT domain. The GAT domain forms three α-helices connected by loops of varying length. The final model is complete except for the N-terminal 26 residues (166–191, dotted line) and the C-terminal 2 residues (304–305), whose electron density is weak. ***b***, Stereo view of the omit $F_o - F_c$ electron density map of the GGA1 N-GAT (Leu178–Asn194) within the ARF1–N-GAT complex. The map was calculated to 1.6 Å resolution and is displayed at 1.5 σ cutoff, superimposed with a ball-and-stick model of the N-GAT domain. ***c***, Stereo view of the ARF1–N-GAT complex. N-GAT forms a helix-loop-helix motif facing switches 1 and 2 of ARF1-GTP. The diagrams in (*a*) and (*c*) are shown in the same orientation, which was chosen by the least-square minimization of the overlap of a common helical region (199–205, shown in red in *a* and *c*) between the GAT domain and the ARF1–N-GAT complex.

Structural changes of GAT upon ARF binding

The structural analysis of the complex between the GAT domain and ARF–GTP required a large number of constructs. Although many GAT domain constructs form stable complexes with ARF–GTP in solution as judged by gel filtration chromatography, numerous crystallization trials did not yield any X-ray–quality of the crystals complex. Therefore, we searched for an optimal length of the GAT domain that would form a stable complex and would form crystals. We found that the bulk of the three-helix bundle prevented crystallization of the complex. A construct truncated at the middle of the long N-terminal helix, N-GAT (166–210), has resulted in a highly stable complex; the crystals of this complex diffracted to 1.6 Å. We first solved the structure of a mutant mouse ARF1 Q71L lacking N-terminal residues 1–7 (Δ17–Q71L) in complex with GTP. We then solved the structure of N-GAT in complex with ARF at 1.6 Å using the molecular replacement method with the structure of mouse ARF–GTP as a search model (Fig. 1*b*). Analysis by surface plasmon resonance (SPR) spectroscopy showed that the binding affinity of N-GAT was almost the same as the entire GGA1-GAT domain (the equilibrium dissociation constants were 1.1 μM for the N-GAT and 1.4 μM for the GGA1-GAT) (Fig. 3*a*,*b*).

The structure of the complex shows that the part of the N-terminal region, which was disordered in the structure of the GGA-GAT domain alone, now forms a helix-loop-helix structure to interact with switches 1 and 2 of ARF–GTP (Fig. 1*c*). In contrast, ARF–GTP does not change its structure upon binding N-GAT (r.m.s. deviation of Cα atoms is 0.6 Å). The interaction between N-GAT and ARF–GTP is predominantly hydrophobic, but there

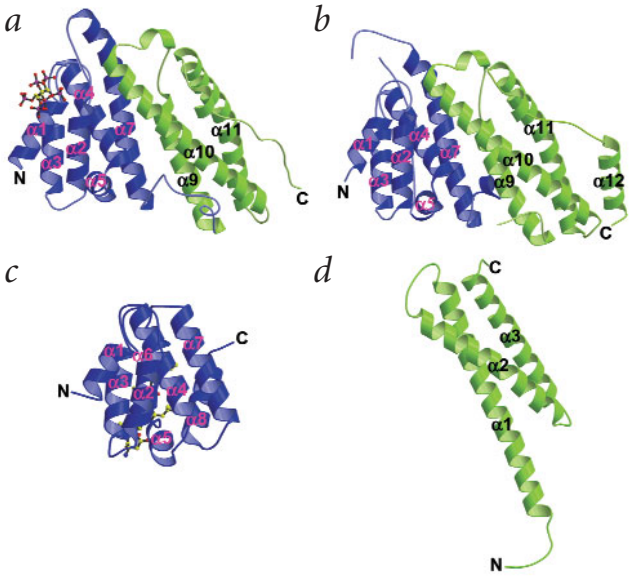

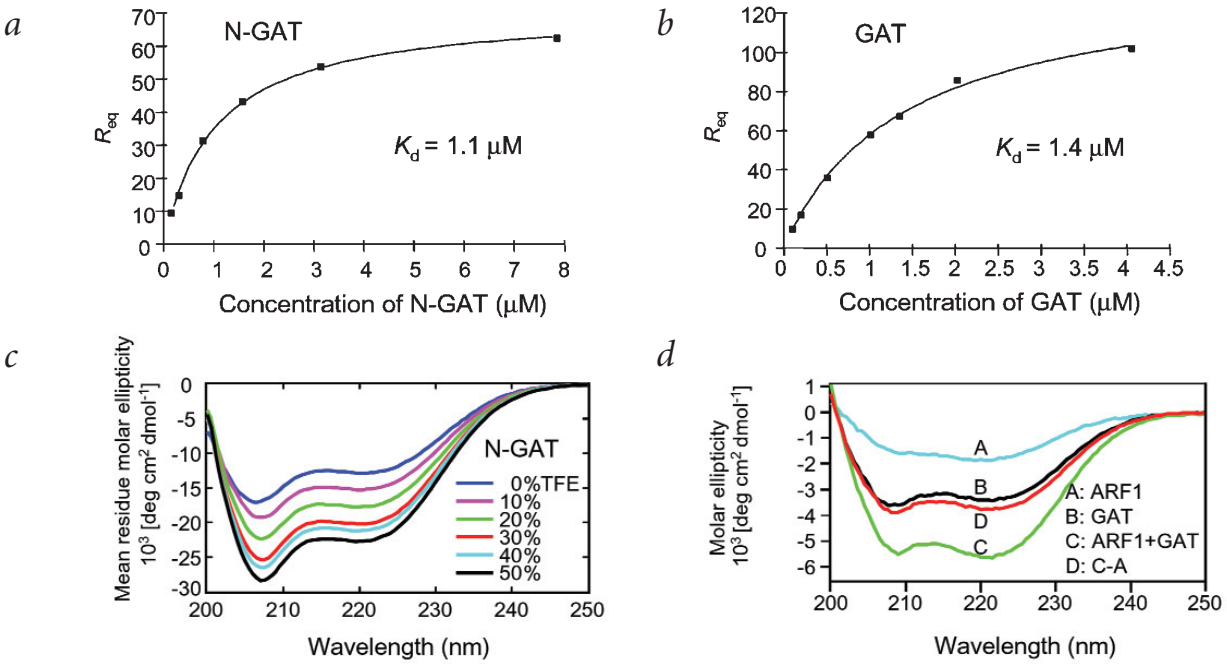

Fig. 3 SPR and CD measurements of N-GAT and GAT domains. ***a***, SPR analysis of the interaction between N-GAT and ARF1Δ17 Q71L. Steady-state resonance (R_{eq}) levels were plotted against N-GAT concentration. ***b***, SPR analysis of the interaction between GAT and ARF1(Δ17–Q71L). Steady-state resonance levels were plotted against GAT concentration. ***c***, CD spectra of N-GAT showing the increase of the α-helical content with the addition of 2,2,2-trifluoroethanol (0–50%). ***d***, GGA1-GAT and ARF1 interaction increases secondary structure content in solution. CD spectra were recorded with ARF1(Δ17–Q71L) (A), GGA1-GAT (B) and a 1:1 mixture of GGA1-GAT and ARF1Δ17 Q71L (C). A difference spectrum (D) of the mixture (C) minus ARF1 (A) shows increased ellipticity compared with the isolated GGA1-GAT domain (B). This is not due to differences in protein concentrations, because the concentration of each protein in the mixture (8 μM) is exactly the same as those of traces A and B within dilution error (see Methods). This observation supports the observation that the region 206–299 of the GGA1-GAT domain forms 3 α-helices when in complex with ARF1.

are three additional hydrogen bonds. The helix-loop-helix is positioned directly against the interswitch region formed by a β-sheet with two antiparallel strands (Fig. 4*a*,*b*). Thus, the structure of the complex supports the notion that the binding of the GGA protein involves both switches 1 and 2 of ARF1–GTP[13,19]. CD spectrum of isolated N-GAT domain showed that it folds partially in solution (Fig. 3*c*). The helical content of isolated N-GAT is estimated at ~43% from the CD spectrum. Addition of 2,2,2-trifluoroethanol, a helix-inducing reagent, to 50% of the entire sample volume increased the helicity of N-GAT to 69%. These values roughly correspond to the helical contents of the corresponding N-GAT portions in the two forms of crystal structures: 27% in the isolated GAT structure (12 out of 45 residues) and 78% in the N-GAT–ARF complex structure (35 out of 45 residues). Taken together, the data indicate that the N-GAT domain alone may only be partially folded in solution, and a significant conformational change of the N-GAT domain occurs upon binding with ARF.

Most of the residues involved in the interaction with ARF (arrowheads, Fig. 4*c*) are conserved in the GAT domains of human GGAs with the exception of Phe169 and Ala179. Furthermore, the X-ray crystal structure of the complex supports previous mutational data by others and us. For example, Asn194 of GGA1 plays an important role in recognition of ARF through two hydrogen bonds between its side chain atoms (Oδ1 and Nδ2) and the main chain nitrogen and oxygen atoms of Phe51^A (where the superscript A denotes a residue of ARF1). This has been clearly demonstrated by the mutational experiments of N194Y[14] and N194A[13]. Furthermore, L178R and V201E mutants lose the ability to bind ARF, presumably because the charged side chains are destabilizing at the hydrophobic interface[14]. Ala193 dose not directly contact ARF in the complex structure, but an A193T mutant abolishes the binding to ARF[14] because the Cβ atom of Ala193 is embedded in the hydrophobic core between the two N-GAT helices and the hydrophilic side chain of threonine will destabilize the complex structure between the A193T mutant and ARF.

Comparison with other ARF-binding proteins

This structure is the first X-ray structure of a complex between ARF and its effector, although structures of complexes either with a GTPase-activating protein, GAP (ARFGAP)[20], or a guanine nucleotide exchange factor, GEF (ARFGEF)[21] have been reported. The manner in which the helix-loop-helix of the N-GAT faces the interswitch region, however, is not shared by ARFGAP or ARFGEF in the structures of the other complexes (Fig. 5*a*–*c*). ARFGAP interacts with switch 2 and α3 of ARF but not with switch 1 (Fig. 5*b*). GGAs and ARFGAPs compete for interaction with ARF1 in its GTP-bound form[13,22]. This observation is supported by the crystal structures of N-GAT–ARF and ARFGAP–ARF (switch 2 is the recognition site for both ARFGAP and GGAs). In the structure of nucleotide-free ARF1 in complex with the Sec7 domain, a GEF for ARF, the latter predominantly interacts with switches 1 and 2 and the α1 region of ARF1 (Fig. 5*c*). The N terminus of helix G in Sec7 binds nucleotide-free ARF near the GTP-binding site, but the N-GAT domain interacts with ARF away from the GTP-binding site. Thus, the GGA protein interacts with ARF in a manner distinct from those of ARFGAP and ARFGEF. There is also a structure reported on the complex between an ARF-like protein, Arl2, whose function remains unclear, and its effector PDEδ[23] (PDB entry 1KSG; Fig. 5*d*). PDEδ interacts with Arl2 in two distinct ways: direct

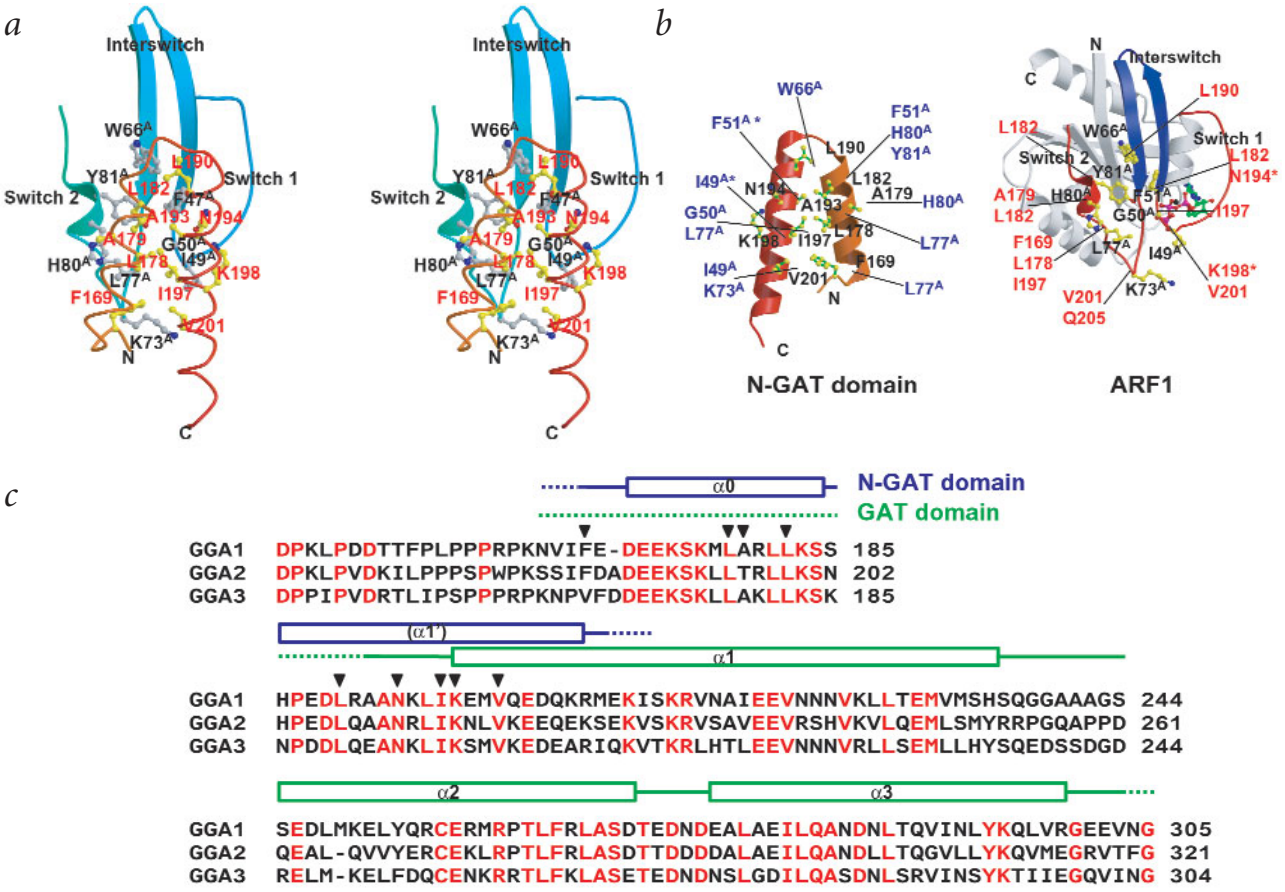

Fig. 4 Interaction between ARF1 and GGA1 N-GAT. ***a***, Stereo diagram of the ARF1–N-GAT interface. Ball-and-stick models in yellow with red labels represent residues of N-GAT which interact with ARF1, and Ala193 which is located in hydrophobic core formed by α0 and α1′. Ball-and-stick models in gray with black labels (also marked with an 'A') show residues of ARF1 that interact with N-GAT. ***b***, ARF1–N-GAT interface shown as an 'open book' representation. The residues involved in the interactions are indicated by ball-and-stick models (bond colors are N-GAT in green and ARF1 in yellow). In the left panel, residues of N-GAT involved in the interaction are labeled in black, and corresponding residues from ARF1 are labeled in blue. The right panel shows the other side of the interaction: ARF1–GTP in ribbon diagram with its residues in the interface labeled in black and corresponding residues of N-GAT in red. Asterisks denote hydrogen-bond interactions. Switches 1 and 2 and the interswitch region of ARF1 are red and blue, respectively. ***c***, Alignment of amino acid sequences of GAT domain from human GGA proteins. Residues conserved in all human GGA proteins are shown in red. Arrowheads indicate GGA1 residues involved in the interaction with the ARF1. The boxes above the sequences depict the secondary structures of GGA1-GAT domain alone (green) and N-GAT domain in the complex with ARF (blue).

hydrophobic interactions between β6 of PDEδ and the Arl2 interswitch region, and an extension of the β-sheet of the interswitch region of Arl2 by the addition of β7 from the effector. Our complex structure shares only part of the first interactions.

GGA recruitment to TGN by ARF

The C-terminal segment of the second helix of the helix-loop-helix motif overlaps with the first part of the long N-terminal helix of the GGA1-GAT structure. By superimposing the common helical segments (residues 199–205) by the least-squares minimization of the Cα atoms (r.m.s. deviation is 0.22 Å), we modeled the structure of the entire GGA1-GAT domain in complex with ARF–GTP. The model consists of four α-helices, which may be considered as part of the putative AP180-like structure. CD experiments of the complex between GGA1-GAT domain and ARF–GTP indicate that GGA1-GAT domain is predominantly α-helical, suggesting that the bulk of α1 and the two helices α2 and α3 are intact even in the complex (Fig. 3*d*). The helical content of GGA1-GAT domain is estimated at ~67% in the free form (Fig. 3*d*, trace B) from the CD spectrum, which increases to 74% upon complex formation with ARF (Fig. 3*d*, trace D). Our combined model of the GAT–ARF complex (Fig. 6) based on the two X-ray structures (Fig. 1*a*,*c*) consists of an 81% helical content (114 out of 140 residues), which corresponds well with the CD measurement. The discrepancy 74% from the CD measurement and 81% and from the X-ray structure could be attributed to the equilibrium between the GAT in complex with ARF (5.3 μM) and the free GAT (2.7 μM) based on the dissociation constant (K_d = 1.4 μM) at the protein concentration of the CD measurement (8 μM).

Our X-ray crystal structures of the GGA1-GAT domain provide a molecular mechanism underlying membrane recruitment of adaptor proteins by ARF–GTP for efficient recruitment of cargo-bound receptors and subsequent formation of clathrin vesicles (Fig. 6). The binding of GGA takes place by adopting the helix-loop-helix motif at the N-terminal of the GAT domain, which docks at switches 1 and 2 with the interswitch region of ARF–GTP on the membrane. This brings the VHS domain of GGA1 closer to the membrane surface, thus making it much easier to recognize signal peptides of cargo proteins such as MPR, sortilin and β-secretase for vesicular transport. The structural change also brings the GGA-VHS domain closer to the C-terminal half of GGA — that is, the hinge region and the ear domain — which might cause an alteration of interactions of GGA with

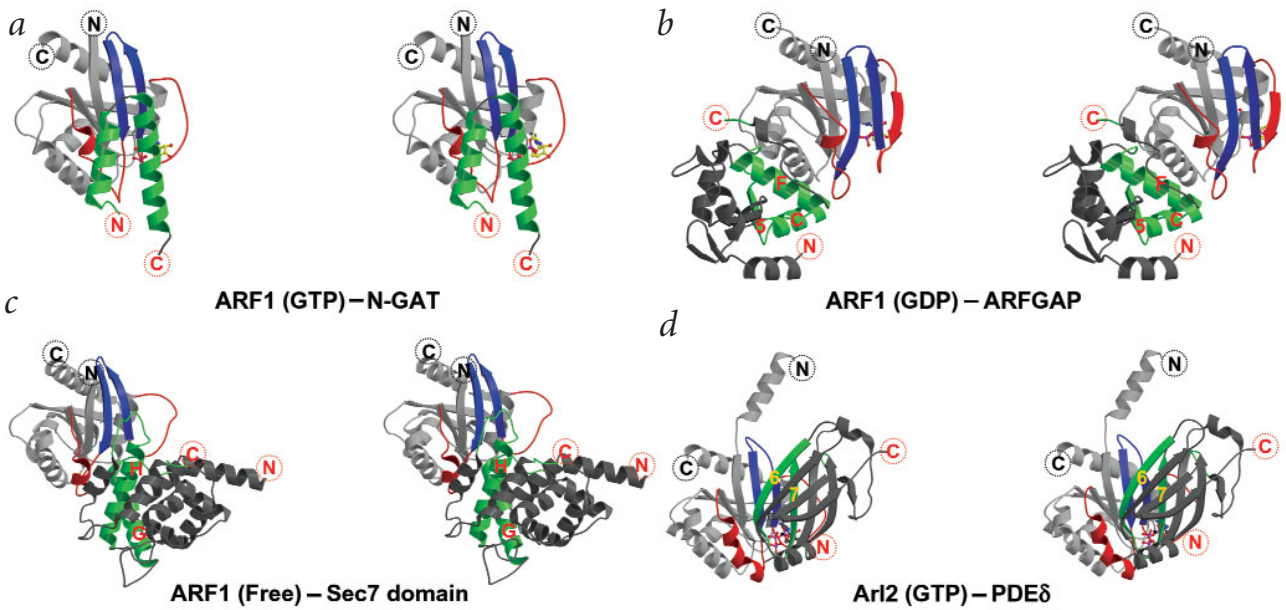

Fig. 5 Comparison of the ARF1–N-GAT complex with other complex structures of ARF and ARF-interacting proteins shown in stereo diagrams: ***a***, the ARF1–N-GAT complex (this work); ***b***, ARF1–ARFGAP complex[20]; ***c***, ARF1–Sec7 domain complex[21]; and ***d***, Arl2–PDEδ complex[23]. The regions of N-GAT that interact with ARF are highlighted in green and the rest in dark gray. The switches 1 and 2, and the interswitch region of ARF are shown in red and blue, respectively, with the rest in light gray. Encircled 'N' and 'C' stand for N and C termini.

clathrin and accessory proteins. In light of the recent finding that the specific sequence of the GGA hinge region is responsible for autoinhibition of the ACLL recognition by the VHS domain[24], further X-ray analysis of this autoinhibited form might result in a structure that may resemble the abovementioned AP180-like super helical structure.

Note added in proof: Collins et al.[25] have published a four-helix structure of the isolated GGA-GAT domain including the N-terminal helix. The comparison of the structures, combined with our CD data, indicates that the isolated GAT domain is in equilibrium between the partially unfolded and folded states and is capable of forming a four-helix structure even in the absence of ARF. The four-helix structure resembles our N-GAT structure in complex with ARF, although the N-terminal helix of the four-helix GAT domain structure is shorter by four residues than that of N-GAT, suggesting stabilization of the helix-loop-helix region of the GGA1-GAT by the interaction with ARF.

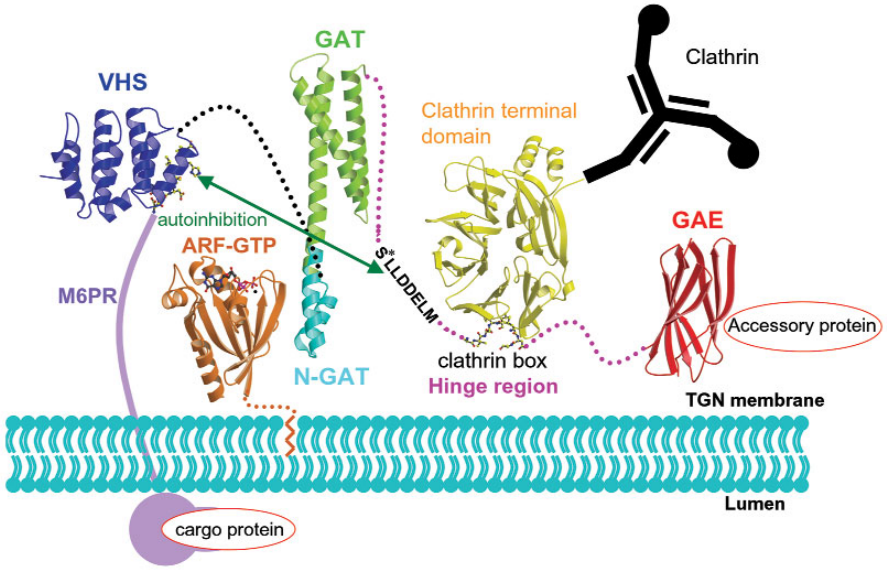

Fig. 6 Domain organization of GGA and a proposed model of the interactions with its partners at several stages of the vesicle formation: M6PR, ARF–GTP, clathrin N-terminal propeller and an accessory protein. The N-terminal VHS domain recognizes the sorting signals, such as M6PR (PDB entry 1JWG). The GAT domain interacts with a membrane-bound ARF (this study). The subsequent hinge region interacts with clathrin (clathrin terminal domain in complex with the clathrin-box peptide from β3-hinge of AP-3; PDB entry 1C9I). The sequence S*LLDDELM interact with VHS domain (autoinhibition), where S* is phosphorylated[24]. Finally, the C-terminal GGA1 GAE domain is modeled from the structure of the ear domain of γ-adaptin (PDB entry 1IU1) based on their similarity both in sequence and function.

Table1 Data collection and refinement statistics

Crystallographic data

Data set	GGA1 GAT domain				ARF1	N-GAT–ARF1
Space group	*R*3				*C*2	$P2_12_12_1$
Unit cell						
a / *b* / *c* (Å)	85.1 / 85.1 / 59.0				127.6 / 50.8 / 52.1	49.4 / 76.9 / 61.9
α / β / γ (°)	90.0 / 90.0 / 120.0				90.0 / 113.4 / 90.0	90.0 / 90.0 / 90.0

Data processing statistics

	GGA1 GAT				ARF1	N-GAT–ARF1
	Native	SeMet-remote	SeMet-peak	SeMet-edge		
Beamline	PF-BL18B	PF-BL18B	PF-BL18B	PF-BL18B	PF-BL6A	PF-BL18B
Wavelength (Å)	1.0	0.9500	0.9806	0.9808	0.977	1.0
Resolution (Å)[1]	30–2.1 (2.21–2.1)	30–2.5 (2.64–2.5)	30–2.5 (2.64–2.5)	30–2.5 (2.64–2.5)	30–1.5 (1.58–1.5)	30–1.6 (1.69–1.6)
Reflections						
Total	64,602	31,814	31,795	31,664	155,298	194,166
Unique	9,302	5.540	5,540	5,536	44,086	30,626
Completeness (%)[1]	100.0 (99.6)	100.0 (100.0)	100.0 (100.0)	100.0 (100.0)	89.8 (62.8)	96.4 (83.1)
R_{merge} (%)[1,2]	4.5 (26.7)	4.9 (18.4)	5.1 (17.5)	4.7 (17.3)	4.3 (20.1)	4.8 (24.5)
I / σ (I)[1]	9.2 (2.8)	5.8 (4.0)	5.9 (4.2)	5.8 (4.1)	12.9 (3.1)	11.0 (3.0)

Phasing statistics

Number of SeMet				
Total	7			
Found	5			
Refined Δf′		–1.026	–3.420	–4.999
Refined f″		3.186	4.121	1.177
FOM	0.54			
FOM after RESOLVE[3]	0.59			

Refinement statistics

	GGA1 GAT	ARF1	N-GAT–ARF1
Resolution (Å)	30–2.1	20–1.5	30–1.6
R_{work}[4]	24.7	19.0	19.8
R_{free}[4]	29.4	21.1	22.7
R.m.s. deviation from ideal values			
Bond length (Å)	0.018	0.008	0.012
Bond angle (°)	1.74	1.23	1.56
Ramachandran plot (%)			
Most favored	85.7	94.3	94.1
Additionally allowed	13.3	5.7	5.9
Generously allowed	1.0	0	0
Disallowed	0	0	0
Number of atoms			
Protein atoms	887	2,664	1,663
Water molecules	108	313	278
GTP atoms	–	64	32
Ions	–	2 (Mg^{2+})	1 (Mg^{2+}), 2 (I^-)
Average *B*-factor (all atoms, Å²)	46.5	13.2	16.8

[1]Values in parentheses are for the highest resolution shell.
[2]$R_{merge} = \Sigma_h\Sigma_j|I_j(h) - \langle I(h)\rangle| / \Sigma_h\Sigma_j I_j(h)$, where $I_j(h)$ is the j^{th} measurement of reflection indices *h* and $\langle I(h)\rangle$ is the mean intensity.
[3]Phasing statistics provided by RESOLVE[29].
[4]*R*-factor $= \Sigma_h||F_o(h)| - |F_c(h)|| / \Sigma_h|F_o(h)|$, and R_{free} was calculated using 5 % of data excluded from refinement.

Methods

Protein expression and purification. Human GGA1-GAT domain (residues 166–305) was cloned into pGEX4T-2 plasmid (Amersham) and expressed as a glutathione *S*-transferase (GST)–fusion protein in *Escherichia coli* BL21 cells. Cells were harvested after induction with 1 mM IPTG for 3 h at 37 °C and lysed by sonication in PBS. The lysate supernatant was loaded on a Glutathione Sepharose 4B column (Amersham). The GST fusion protein was eluted by glutathione and cleaved by thrombin. Ammonium sulfate was added to a final concentration of 2 M to precipitate the cleaved GAT domain. The protein was dissolved in 100 mM NaCl and 20 mM Tris-HCl, pH 8.0, and further purified by Superdex 75 (Amersham) gel filtration column chromatography. The eluted GGA1 GAT domain was dialyzed against 1 mM Tris-HCl, pH 8.0, and concentrated to ~10 mg ml^{-1}. SeMet-substituted protein was expressed in *E. coli* DL41 cells and purified by the same procedure as the native protein. Mouse ARF1 Q71L mutant lacking N-terminal residues 1–17 (Δ17–Q71L) was cloned into pProEX HT plasmid (Life Technologies) and expressed as a His_6-tagged protein in *E. coli* BL21 cells. Cells were harvested after induction with 0.1 mM IPTG for 6 h at 25 °C and lysed by sonication

in 100 mM NaCl, 5 mM $MgCl_2$ and 20 mM Tris-HCl, pH 8.0. After purification by a Ni-NTA affinity column, the His_6-tag was removed by Tobacco Etch Virus (TEV) protease (Invitrogen). ARF1 was further purified by gel filtration column chromatography and dialyzed against 5 mM $MgCl_2$ and 10 mM Tris-HCl, pH 8.0, and concentrated to ~10 mg ml^{-1}. For purification of the ARF1–N-GAT domain complex, the N-terminal 45 residues of the GGA1 GAT domain (residues 166–210) were cloned into pGEX4T-2 (Amersham) and expressed in *E. coli* BL21 cells. The GST-N-GAT fusion protein was loaded on a Glutathione Sepharose 4B column. Then purified ARF1(Δ17–Q71L) was loaded on the column. The ARF1–GST-N-GAT complex was eluted by glutathione and cleaved by thrombin to remove GST, and further purified by gel filtration column chromatography. The ARF1–N-GAT complex was dialyzed against 5 mM $MgCl_2$ and 10 mM Tris-HCl, pH 8.0, and concentrated to ~30 mg ml^{-1}.

Crystallization. Crystallization conditions for the GAT domain, ARF1(Δ17–Q71L) and the N-GAT–ARF1(Δ17–Q71L) complex were screened using the hanging drop vapor diffusion method at 293 K. GAT domain crystals were obtained after 2 d against a reservoir containing 35% (v/v) MPD, 2% (w/v) PEG 6000 and 0.1 M Tris-HCl, pH 7.5. The SeMet-substituted GAT domain was crystallized in almost the same condition as that of the native GAT domain. ARF1 crystals were obtained after 2 d against a reservoir containing 24% (v/v) PEG 3350, 0.2 M ammonium acetate and 0.1 M acetate buffer, pH 4.0. N-GAT–ARF1 complex crystals were obtained after 2 d against a reservoir containing 10% (v/v) PEG 3350, 0.2 M KI.

X-ray data collection and processing. The crystals of GGA1 GAT domain were picked up from the droplets with cryo-loops and directly frozen into liquid nitrogen. For crystal structure analysis, native data set was collected at 100 K with synchrotron radiation (1.0 Å wavelength) at beamline 18B of the Photon Factory (PF), High Energy Accelerator Research Organization (KEK), Tsukuba, Japan. The native crystal belongs to the rhombohedral space group *R*3 with unit cell dimensions $a = 85.1$, $c = 59.1$ Å, $\alpha = 90$ and $\gamma = 120°$. Three data sets of the crystal of SeMet GAT domain (λ_{peak} = 0.9806 Å, λ_{edge} = 0.9808 Å and λ_{remote} = 0.9500 Å) were collected at 2.5 Å resolution. Diffraction images of the native and SeMet crystals were processed with DPS/MOSFILM[26] and scaled with SCALA[27]. The data set of ARF(Δ17–Q71L) was collected at 100 K with synchrotron radiation (0.977 Å wavelength) at beamline 6A of the Photon Factory (PF). The ARF1 crystal belongs to the monoclinic space group *C*2 with unit cell dimensions of $a = 127.6$, b=50.8, $c = 52.1$ Å and $\beta = 113.4°$. The ARF1–N-GAT domain complex data set was collected at 100 K with synchrotron radiation (1.0 Å wavelength) at beamline 18B of the Photon Factory (PF). The ARF1–N-GAT domain complex crystal belongs to the orthorhombic space group $P2_12_12_1$ with unit cell dimensions of $a = 49.4$, $b = 76.9$ and c = 61.9 Å. The data collection and final processing statistics are summarized in Table 1.

Structure determination and refinement. The crystal structure of human GGA1-GAT domain was solved using the MAD method with the crystal of SeMet-substituted protein. SOLVE[28] was used in combination to locate and refine five of the seven Se sites, and RESOLVE[29] was used for solvent flattening, assuming a 55% solvent content. An initial model was generated by Arp/Warp[30] and refined using CNS[31] and REFMAC5 (ref. 32). The final model (with 108 water molecules) refined to 30.0–2.1 Å resolution has an *R*-factor of 24.7% and an R_{free} of 29.4%. The crystal structure of ARF1(Δ17–Q71L) was solved using molecular replacement method using AmoRe[33] and the human ARF6 complex with GTPγS (PDB entry 1HFV, GTP form) as a search model. The current model (with 313 water molecules) refined using CNS[31] and REFMAC5 (ref. 32) for the resolution range from 30.0–1.5 Å has an *R*-factor of 19.0% and an R_{free} of 21.1%. The crystal structure of human GGA1 N-GAT domain–ARF1(Δ17–Q71L) was solved by the molecular replacement method using AMoRe[33] and the human ARF1–GTP form as a search model. The initial electron density map at GGA1 N-GAT domain region was clear, and we could build an initial model of the N-GAT domain using ARP/wARP[30]. The current model (with 278 water molecules) refined using CNS[31] and REFMAC5 (ref. 32) for the resolution range 30.0–1.6 Å has an *R*-factor of 19.8% and an R_{free} of 22.7%. The final refinement statistics are shown in Table 1. Figures were produced using MolScript[34], Raster3D[35] and CONSCRIPT[36].

CD and SPR measurements. CD spectra were recorded on a Jasco J-820 spectropolarimeter at 25 °C in a cuvette with 1 mm path length. N-GAT spectra (Fig. 3*c*) were recorded with the protein concentration of 80 μM in PBS buffer. GAT–ARF spectra (Fig. 3*d*) were recorded in 20 mM Tris-HCl, pH8.0, 100 mM NaCl and 5 mM $MgCl_2$. For each spectrum of GAT and ARF, the stock solutions of GAT and ARF (prepared at 0.078 mM and 0.15 mM, respectively) were diluted with buffer up to 250 μl for the final protein concentration of 8 μM (that is, for GAT, 25 μl stock solution plus 225 μl buffer, and for ARF, 13 μl stock solution plus 237 μl buffer). For the spectrum of the GAT–ARF complex, 25 μl GAT stock solution, 13 μl ARF stock solution and 212 μl buffer were mixed to obtain the final concentrations of 8 μM each. Therefore, each protein concentration of the mixture (Fig. 3*d*, trace C) was exactly the same as the individual solution (Fig. 3*d*, traces A and B), and the difference between traces B and D in Fig. 3*d* is larger than the dilution error. Helical content was estimated using SELCON2 (self consistent method release 2)[37] within the DICROPROT package (*http://pbil.ibcp.fr*).

SPR spectra were analyzed by BIAcore 2000. His_6-tagged ARF1(Δ17–Q71L) was captured on a sensor chip NTA. Binding of GAT and N-GAT domains to ARF was analyzed in 20 mM Tris-HCl, pH 8.0, 100 mM NaCl, 5 mM $MgCl_2$ and 1 mM DTT at a flow rate of 20 μl min^{-1} at 25 °C. Sensorgrams were analyzed using the BIAevaluation 3.2. K_d values were determined using the steady-state affinity model by plotting steady-state resonance (R_{eq}) levels against protein concentrations.

Coordinates. The coordinates have been deposited in the Protein Data Bank (accession codes 1J2H for human GGA1 GAT domain, 1J2I for ARF1(Δ17–Q71L) and 1J2J for the ARF1(Δ17–Q71L)–N-GAT domain complex).

Acknowledgments

Coordinates of the two complex structures, ARF–ARFGAP and ARF–Sec7 domain, were provided by J. Goldberg. This work was supported in part by Grants-in-Aid for Scientific Research from the Ministry of Education, Culture, Sports, Science and Technology (MEXT) of Japan, from the Japan Society for Promotion of Science (fellowship to H.T.), from the University of Tsukuba Research Projects, and by Protein 3000 Project of the MEXT.

Competing interests statement

The authors declare that they have no competing financial interests.

Received 21 January, 2003; accepted 19 March, 2003.

1. Robinson, M.S. & Bonifacino, J.S. Adaptor-related proteins. *Curr. Opin. Cell Biol.* **13**, 444–453 (2001).
2. Boman, A.L., Zhang, C.-J., Zhu, X. & Kahn, R.A. A family of ADP-ribosylation factor effectors that can alter membrane transport through the *trans*-Golgi. *Mol. Biol. Cell* **11**, 1241–1255 (2000).
3. Dell'Angelica, E.C. *et al*. GGAs: a family of ADP ribosylation factor-binding proteins related to adaptors and associated with the Golgi complex. *J. Cell Biol.* **149**, 81–93 (2000).
4. Hirst, J., Lui, W.W., Bright, N.A., Totty, N., Seaman, M.N. & Robinson, M.S. A family of proteins with γ-adaptin and VHS domains that facilitate trafficking between the *trans*-Golgi network and the vacuole/lysosome. *J. Cell Biol.* **149**, 67–79 (2000).
5. Poussu, A., Lohi, O. & Lehto, V.-P. Vear, a novel Golgi-associated protein with VHS and γ-adaptin "ear" domains. *J. Biol. Chem.* **275**, 7176–7183 (2000).
6. Takatsu, H., Yoshino, K. & Nakayama, K. Adaptor γ ear homology domain conserved in γ-adaptin and GGA proteins that interact with γ-synergin. *Biochem. Biophys. Res. Commun.* **271**, 719–725 (2000).
7. Nielsen, M.S. *et al*. The sortilin cytoplasmic tail conveys Golgi-endosome transport and binds the VHS domain of the GGA2 sorting protein. *EMBO J.* **20**, 2180–2190 (2001).
8. Puertollano, R., Aguilar, R.C., Gorshkova, I., Crouch, R.J. & Bonifacino, J.S. Sorting of mannose 6-phosphate receptors mediated by the GGAs. *Science* **292**, 1712–1716 (2001).
9. Zhu, Y., Doray, B., Poussu, A., Lehto, V.-P. & Kornfeld, S. Binding of GGA2 to the lysosomal enzyme sorting motif of the mannose 6-phosphate receptor. *Science* **292**, 1716–1718 (2001).
10. Takatsu, H., Katoh, Y., Shiba, Y. & Nakayama, K. Golgi-localizing, γ-adaptin ear homology domain, ADP-ribosylation factor-binding (GGA) proteins interact with acidic dileucine sequences within the cytoplasmic domains of sorting receptors through their Vps27p/Hrs/STAM (VHS) domains. *J. Biol. Chem.* **276**, 28541–28545 (2001).
11. Doray, B., Ghosh, P., Griffith, J., Geuze, H.J. & Kornfeld, S. Cooperation of GGAs and AP-1 in packaging MPRs at the *trans*-Golgi network. *Science* **297**, 1700–1703 (2002).
12. Zhdankina, O., Strand, N.L., Redmond, J.M. & Boman, A.L. Yeast GGA proteins interact with GTP-bound Arf and facilitate transport through the Golgi. *Yeast* **18**, 1–18 (2001).
13. Puertollano, R., Randazzo, P.A., Presley, J.F., Hartnell, L.M. & Bonifacino, J.S. The GGAs promote ARF-dependent recruitment of clathrin to the TGN. *Cell* **105**, 93–102 (2001).
14. Takatsu, H., Yoshino, K., Toda, K. & Nakayama, K. GGA proteins associate with Golgi membranes through interaction between their GGAH domains and ADP-ribosylation factors. *Biochem. J.* **365**, 369–378 (2002).
15. Ford, M.G. *et al.* Simultaneous binding of PtdIns(4,5)P_2 and clathrin by AP180 in the nucleation of clathrin lattices on membranes. *Science* **291**, 1051–1055 (2001).
16. Mao, Y., Chen, J., Maynard, J.A., Zhang, B. & Quiocho, F.A. A novel all helix fold of the AP180 amino-terminal domain for phosphoinositide binding and clathrin assembly in the synaptic vesicle endocytosis. *Cell* **104**, 433–440 (2001).
17. Misra, S., Puertollano, R., Kato, Y., Bonifacino, J.S. & Hurley, J.H. Structural basis for acidic-cluster-dileucine sorting-signal recognition by VHS domains. *Nature* **415**, 933–937 (2002).
18. Shiba, T. *et al.* Structural basis for recognition of acidic-cluster dileucine sequence by GGA1. *Nature* **415**, 937–941 (2002).
19. Kuai, J., Boman, A.L., Arnold, R.S., Zhu, X. & Kahn, R.A. Effects of activated ADP-ribosylation factors on Golgi morphology require neither activation of phospholipase D1 nor recruitment of coatomer. *J. Biol. Chem.* **275**, 4022–4032 (2000).
20. Goldberg, J. Structural and function analysis of the ARF1-ARFGAP complex reveals a role for coatomer in GTP hydrolysis. *Cell* **96**, 893–902 (1999).
21. Goldberg, J. Structural basis for activation of ARF GTPase: mechanisms of guanine nucleotide exchange and GTP-myristoyl switching. *Cell* **95**, 237–248 (1998).
22. Jacques, K.M. *et al.* Arf1 dissociates from the clathrin adaptor GGA prior to being inactivated by Arf GTPase-activating proteins. *J. Biol. Chem.* **277**, 47235–47241 (2002).
23. Hanzal-Bayer, M., Renault, L., Roversi, P., Wittinghofer, A. & Hillig, R.C. The complex of Arl2-GTP and PDEδ: from structure to function. *EMBO J.* **21**, 2095–2106 (2002).
24. Doray, B., Bruns, K., Ghosh, P. & Kornfeld, S. Autoinhibition of the ligand-binding site of GGA1/3 VHS domains by an internal acidic cluster-dileucine motif. *Proc. Natl. Acad. Sci.* **99**, 8072–8077 (2002).
25. Collins, B.M., Watson, P.J. & Owen, D.J. The structure of the GGA1-GAT domain reveals the molecular basis for ARF binding and membrane association of GGAs. *Dev. Cell* **4**, 321–332 (2003).
26. Leslie, A.W.G. *Joint CCP4 and ESF-EACMB Newsletter on Protein Crystallography* Vol. 26 (Daresbury Laboratory, Warrington, 1992).
27. Evans, P.R. *Proceedings of the CCP4 Study Weekend on Data Collection & Processing* (eds. Sawyer, L., Isaacs, N. & Bailey, S.) 114–122 (Daresbury Laboratory, Warrington; 1993).
28. Terwilliger, T.C. & Berendzen, J. Automated MAD and MIR structure solution. *Acta Crystallogr. D* **55**, 849–861 (1999).
29. Terwilliger, T.C. Maximum-likelihood density modification. *Acta Crystallogr. D* **56**, 965–972 (2000).
30. Perrakis, A., Morris, R. & Lamzin, V.S. Automated protein model building combined with iterative structure refinement. *Nature Struct. Biol.* **6**, 458–463 (1999).
31. Brunger, A.T. *et al.* Crystallography & NMR system: a new software suite for macromolecular structure determination. *Acta Crystallogr. D* **54**, 905–921 (1998).
32. Murshudov, G.N., Vagin, A.A. & Dodson, E.J. Refinement of macromolecular structures by the maximum-likelihood method. *Acta Crystallogr. D* **53**, 240–255 (1997).
33. Navaza, J. AMoRE — an automated package for molecular replacement. *Acta Crystallogr. A* **50**, 157–163 (1994).
34. Kraulis, P.J. MOLSCRIPT: a program to produce both detailed and schematic plots of protein structures. *J. Appl. Crystallogr.* **24**, 946–950 (1991).
35. Merritt, E.A. & Bacon, D.J. Raster3D: photorealistic molecular graphics. *Methods Enzymol.* **277,** 505–524 (1997).
36. Lawrence, M.C. & Bourke, P. CONSCRIPT: a program for generating electron density isosurfaces for presentation in protein crystallography. *J. Appl. Crystallogr.* **33**, 990–991 (2000).
37. Sreerama, N. & Woody, R.W. A self-consistent method for the analysis of protein secondary structure from circular dichroism. *Anal. Biochem.* **209**, 32–44 (1993).